JDDB, 2(1), 01-09, 2024
https://doi.org/10.58985/jddb.2024.v02i01.08
ISSN(Print):2959-3123

Journal of Drug Designing & Bioinformatics

*Research Article*

# Site Identification by Ligand Competitive Saturation (SILCS) Based Design and Synthesis of Novel Allosteric Inhibitors of Protein Tyrosine Phosphatase 1B (PTP 1B).

**Atef Abdel-Monem Abdel-Hafez Abdel-Galil** [1, 2*]

1. Department of Medicinal Chemistry, Faculty of Pharmacy, Assiut University, Assiut, 71526, Egypt.
2. Department of Medicinal Chemistry and Pharmacognosy, College of Pharmacy, Qassim University, Buraidah 51452, Saudi Arabia

***Article Information***
*Received:* 29 November 2023
*Revised:* 20 December 2023
*Accepted:* 21 December 2023
*Published:* 02 January 2024

***Academic Editor***
Prof. Dr. Samir Chtita

***Corresponding Author***
Atef Abdel-Monem Abdel-Hafez Abdel-Galil
E-mail:
a.abdelgalil@qu.edu.sa,
aaahafez66@gmail.com
Tel: +966557663046

***Keywords***
Site identification by ligand competitive saturation (SIL CS), allosteric inhibitors, protein tyrosine phosphatase 1B, insulin-resistance type 2 diabetes mellitus.

## Abstract

As a negative regulator of the insulin signaling pathways, protein tyrosine phosphatase 1B (PTP 1B) has currently been thought to be a validated druggable target for the development of new treatment options intended to treat insulin-resistant type 2 diabetes mellitus (IR-T2DM). In this study, we design and synthesize inhibitors targeting the allosteric PTP1B site by using novel computer-aided drug design methodology site identification of ligand competitive saturation (SLICS). A novel series of 5-(*N*-substituted)-2-(2,5-dimethyl-1*H*-pyrrol-1-yl) benzoic acid derivatives (**3a-g**) were designed by using SILCS based on functional group affinity patterns in the form of free energy maps that may be used to compute protein-ligand binding poses and affinities. The designed compounds (**3a-g**) were synthesized and their structures were confirmed by IR, $^{1}$H, and $^{13}$C-NMR in addition to HR-MS. Visualization of SILCS FragMaps reveals the favorable and unfavorable sites for functional group interactions with PTP 1B protein. 5-(Cyclopropylamino)-2-(2,5-dimethyl-1*H*-pyrrol-1-yl) benzoic acid **3e** was the most docked compound with the highest free ligand-free energy (generic -24.883 kcal mol$^{-1}$ and specific -24.364 kcal mol$^{-1}$). Findings from this study strongly suggest benzoic acid derivative **3e** as a lead compound against PTP 1B for the management of T2DM.

## 1. Introduction

Cellular pathways regulated by tyrosine phosphorylation offer a rich source of drug targets for developing novel therapeutics [1]. Over the past decades, a huge effort has been undertaken by academia and the pharmaceutical industry to target kinases as well as phosphatases with small molecules. These efforts have been remarkably more successful for kinases, resulting in more than 25 kinase inhibitors being approved for clinical use and many more in clinical trials [2]. On the other hand, not a single phosphatase inhibitor has been submitted to the clinic. Because at the molecular level, there are significantly more kinases (> 500) than phosphatases (>130) encoded in the human genome, so as to say that the substrate specificity of phosphatases is much broader. Secondly, the substrate pocket of phosphatases is positively charged to complement the high negative charge of phosphorylated substrate which leads to the predominant discovery of negatively charged substrate, which suffers from poor bioavailability [2].

One way to circumvent these issues is the identification of allosteric sites that are less conserved. Using novel computer-aided drug design methodology site identification by ligand competitive saturation (SILCS), a novel allosteric site in PTP 1B between $\alpha$3 and $\beta$6 located 20 Å from the active site was identified [3]. Utilizing a combined grand canonical Monte Carlo (GCMC) molecular dynamics (MD) sampling of multiple co-solvent or solute molecules representing different functional groups against a particular target protein in an aqueous solution, the SILCS methodology is a co-solvent sampling technique used to compute functional group binding affinity patterns. The simulations yield functional group probability distributions, that are then transformed into free energy maps, or "FragMaps," which help find new compounds or drugs that enhance ligand binding affinity. Furthermore, fragment-based drug design, protein-protein interactions, pharmacophore screening, and excipient evaluation in the formulation of biologics are all possible to benefit from the application of FragMaps [4]. This allosteric site is not highly conserved among phosphatases, thus providing an opportunity to circumvent the selectivity problem associated with the active-site targeting inhibitors. One small molecule, compound **P58** (Table 1), has been identified to bind to this site and inhibit the activity of the enzyme by blocking the mobility of the catalytically critical WPD loop. However, **P58** suffers from significant limitations such as weak potency ($IC_{50}$ 10 μM) and poor chemical stability. Using SILCS methodology, an additional hydrophobic pocket adjacent to the aromatic pocket occupied by **P58** was characterized which over to improve the affinity [5]. Motivated by the success of **P58**, the new inhibitors would keep the overall configuration and hydrogen bonding potential of the OH group and provide an additional hydrophobic interaction that will interact favorably with PTP 1B, and thus, further improve the potency of the inhibitors. Preliminary CADD using SILCS suggests that the target compounds will adopt a position and orientation similar to that of **P58** in its complex with PTP 1B. The ligand grid-free energies resulting from docking of the designed inhibitors favored the addition of the hydrophobic motifs such as methyl propyl, isopropyl, butyl, cyclopropyl, cyclopropylmethyl, and cyclohexylmethyl moieties to position 5 of **P58** rather than position 1. Based on the above-mentioned ideas, novel 5-(*N*-substituted)-2-(2,5-dimethyl-1*H*-pyrrol-1-yl) benzoic acid candidates (**3a-g**) were designed and synthesized as promising PTP1B inhibitors.

## 2. Materials and Methods

### *2.1 Computational methodology*

PTP1B allosteric site identified and characterized by Mackerell *et al.* [10] using the site identification by ligand competitive saturation hotspot approach (SILCS-Hotspot) was employed in this study. By manually aligning the ligands (**P58**, **2**, **3a-g**, and **4-11**) with crystal structure ligand orientations with the highest common substructure in MOE (Chemical Computing Group), the ligands were created. The total of the atomic GFE scores derived from the categorization of every atom in a ligand and its overlap with the associated FragMap is known as the ligand grid free energy, or LGFE. The ligand position and conformation should be sampled using Monte Carlo methods (referred to as SILCS-MC) using the LGFE score and the ligand intramolecular energy as the Metropolis criteria. Translations, rigid-body rotations, and rotations of dihedrals about rotatable bonds are the movements used in SILCS-MC. Sampling the ligand-binding conformation in the field of the FragMaps in conjunction with the SILCS is the primary goal. The protein's prohibited area, known as the exclusion map, is where no water or non-hydrogen solute sample was found during the SILCS simulations. The GFE energy of ligand non-hydrogen atoms that overlap with the exclusion maps is 1000 kcal mol-1. For the SILCS-MC simulations, we apply an extensive docking protocol in this work, where the ligand is randomly oriented and positioned within a user-defined radius [10]. This process has the advantage of allowing for a greater conformational space exploration within the binding pocket. In order to achieve the ideal configuration, the SILCS-MC process starts with 10,000 steps of energy reduction of the ligand structures. This is followed by 10,000 steps of regular MC and 40,000 steps of annealing. For the standard MC, the temperature was set to 300 K, and for the annealing stages, it was progressively dropped to 0 K. The most advantageous LGFE scores, which are then utilized exclusively for ligand scoring, are employed to determine the final ligand binding


https://doi.org/10.58985/jddb.2024.v02i01.08

**Table 1.** The LGFE binding scores of 5-(substituted)-2-(2,5-dimethyl-1H-pyrrol-1-yl) benzoic acid derivatives (**P58**, **2**, **3a-g** and **4-11**) with allosteric site of PTP1B using SILCS methodology.

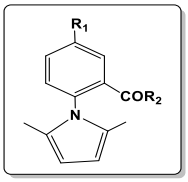


| Entry | AT No. | $R_1$ | $R_2$ | FragMap (PTP 1B) LGFE Generic | FragMap (PTP 1B) LGFE Specific | FragMap (TCPTP) LGFE Generic | FragMap (TCPTP) LGFE Specific | FragMap (PTP 1B) LGFE Generic difference | FragMap (TCPTP) LGFE Specific difference |
|---|---|---|---|---|---|---|---|---|---|
| P58 | 1001 | OH | OH | -22.086 | -21.229 | -16.782 | -15.401 | -5.304 | -5.828 |
| 2 | 1002 | Br | OH | -22.126 | -21.284 | -16.580 | -14.633 | -5.546 | -6.651 |
| 3a | 1003 | Ethylamino | OH | -23.997 | -23.453 | -19.357 | -16.887 | -4.64 | -6.566 |
| 3b | 1004 | Propylamino | OH | -24.068 | -24.154 | -20.703 | -17.738 | -3.365 | -6.416 |
| 3c | 1005 | Isopropyl-amino | OH | -23.402 | -21.296 | -21.814 | -19.442 | -1.588 | -1.854 |
| 3d | 1006 | Butylamino | OH | -24.358 | -23.894 | -20.578 | -17.256 | -3.78 | -6.638 |
| 3e | 1007 | Cyclopropyl-amino | OH | -24.883 | -24.364 | -20.854 | -17.289 | -4.029 | -7.075 |
| 3f | 1008 | Cyclopropyl-methylamino | OH | -24.159 | -23.690 | -22.207 | -19.854 | -1.952 | -3.836 |
| 3g | 1009 | Cyclohexyl-methylamino | OH | -24.579 | -22.589 | -25.414 | -24.870 | 0.835 | 2.281 |
| 4 | 1010 | Br | $OCH_3$ | -21.224 | -20.551 | -16.621 | -15.301 | -4.603 | -5.25 |
| 5 | 1011 | Br | Ethylamino | -20.271 | -19.917 | -16.071 | -15.627 | -4.2 | -4.29 |
| 6 | 1012 | Br | Propylamino | -20.124 | -19.535 | -16.685 | -16.161 | -3.439 | -3.374 |
| 7 | 1013 | Br | Isopropylamino | -20.313 | -19.385 | -17.936 | -17.749 | -2.377 | -1.636 |
| 8 | 1014 | Br | Butylamino | -20.032 | -19.537 | -17.268 | -16.131 | -2.764 | -3.406 |
| 9 | 1015 | Br | Cyclopropyl-amino | -20.394 | -21.048 | -17.406 | -16.646 | -2.988 | -4.402 |
| 10 | 1016 | Br | Cyclopropyl-methylamino | -20.987 | -21.766 | -17.855 | -17.987 | -3.132 | -3.779 |
| 11 | 1017 | Br | Cyclohexyl-methylamino | -21.425 | -20.859 | -21.698 | -23.303 | 0.273 | 2.444 |

conformations. For every ligand, we run five independent simulations with a minimum of 50 MC runs each. The simulation proceeded to a maximum of 250 MC runs before stopping once the three most favorable LGFE scores within 0.5 kcal mol-1 criteria were met or the most favorable LGFE score used from the 250 MC runs. The simulation was stopped after 50 MC runs if the three most favorable LGFE scores were within 0.5 kcal mol-1. This procedure was employed to enhance the overall sampling and find the minimum free energy binding conformation. The most favorable LGFE score and associated ligand conformation were then selected from the five independent simulations. Further details about the rapid and accurate estimation of protein–ligand relative binding affinities using site identification by ligand competitive saturation were described by Mackerell *et al.* [10].

### *2.2 Chemistry part*

All $^{1}$H-NMR and $^{13}$C-NMR spectra were recorded on spectrophotometers operating at 400 MHz and 100 MHz, respectively. Chemical shifts (δ) are expressed in ppm, and coupling constants *J* are given in hertz. Chemical shifts are reported relative to residual solvent peak (DMSO-*d6* at 2,5 ppm for $^{1}$H and 39.51 ppm for $^{13}$C). The following abbreviations were used for signal multiplicity: s = singlet, brs = broad singlet, d = doublet, dd = doublet of doublet, t = triplet, q = quartet, m = multiplet. Column chromatography purifications were conducted on silica gel 60 Å (40-63 µm, Sorbent Technologies), Analytical thin layer chromatography (TLC) was carried out on glass sheets Precoated with silica get (60 UV 254, Sorbent Technologies). Mass spectra were recorded using



*https://doi.org/10.58985/jddb.2024.v02i01.08*

electrospray as the ionization technique. 5-Bromo-2-(2, 5-Dimethyl-1*H*-pyrrol-1-yl) benzoic acid **2** was obtained by treatment of 1 with excess amount of 2, 5-hexanedione without solvent, and its structure was confirmed by reported data [13].

*2.2.1 General method for synthesis of the target compounds (3a-g)*

A mixture of an aryl bromide **2** (294 mg, 1 mmol), Cu(I)I (39 mg, 0.2 mmol), and $K_2CO_3$ (207.5 mg, 1.5 mmol) was dissolved in $CH_3CN$: $H_2O$ mixture ([1:4, v/v, 2.5 mL). The amine (3 mmol) was added and the reaction mixture was sealed in a 20 mL screwed tube and stirred electromagnetically in an oil bath at 100~130 °C from 24~36 hrs. The reaction mixture was cooled at room temperature, and diluted with $H_2O$ (20 mL), and the pH was adjusted to 3~4 with 1*N* HCl. The water phase was extracted with $CH_2Cl_2$ (3 × 30 mL) and the combined organic phase was dried over $MgSO_4$. The Organic solvent was removed and purified by silica gel column chromatography (eluent: 2% methanol in $CH_2Cl_2$) to give the pure product.

*2-(2,5-Dimethyl-1H-pyrrol-1-yl)-5-(ethylamino) benzoic acid (**3a**)*

Pale yellow oil (0.199 g, 77 %), $^1$H-NMR δ 0.71-0.76 (t, *J* = 6.8 Hz, 3H), 1.74 (s, 6H), 2.86-2.90 (q, *J* = 6.8 Hz, 2H), 5.58 (s, 2H), 6.02 (brs, 1H), 6.61-6.64 (dd, *J* = 8.8, 2.4 Hz, 1H), 6.78-6.81 (d, *J* = 8.8 Hz, 1H), 6.88-6.90 (d, *J* = 2.4 Hz, 1H), 12.38 (brs, 1H). $^{13}$C-NMR δ 17.09, 21.92, 40.71, 104.91, 112.60, 114.50, 124.86, 128.60, 131.00, 132.81, 149.93, 169.63. ESI-MS m/z 259 $(M + H)^+$ calculated for $C_{15}H_{18}N_2O_2$.

*2-(2,5-Dimethyl-1H-pyrrol-1-yl)-5-(propylamino) benzoic acid (**3b**)*

Pale yellow oil (0.193 g, 71 %), $^1$H-NMR δ 0.78-0.81 (t, *J* = 6.8 Hz, 3H), 1.32-1.37 (m, 2H), 1.75 (s, 6H), 2.91-2.96 (q, *J* = 6.8 Hz, 2H), 5.60 (s, 2H), 6.05 (brs, 1H), 6.69-6.72 (dd, *J* = 8.8, 2.4 Hz, 1H), 6.83-6.85 (d, *J* = 8.8 Hz, 1H), 6.92-6.93 (d, *J* = 2.4 Hz, 1H), 12.41 (brs, 1H). $^{13}$C-NMR δ 11.81, 13.03, 22.82, 40.74, 104.91, 112.60, 114.50, 124.86, 128.60, 131.00, 132.81, 149.93, 169.33. ESI-MS m/z 273 $(M + H)^+$ calculated for $C_{16}H_{20}N_2O_2$.

*5-(Isopropylamino)-2-(2,5-dimethyl-1H-pyrrol-1-yl) benzoic acid (**3c**)*

Pale yellow oil (0.201 g, 74 %), $^1$H-NMR δ 1.16-1.18 (d, *J* = 6.0 Hz, 6H), 1.76 (s, 6H), 3.75 (m, 1H), 5.65 (s, 2H), 6.95 (brs, 1H), 6.72-6.75 (dd, *J* = 8.4, 2.4 Hz, 1H), 6.88-6.90 (d, *J* = 8.4 Hz, 1H), 6.95-6.96 (d, *J* = 2.4 Hz, 1H), 12.52 (brs, 1H). $^{13}$C-NMR δ 17.85, 27.56, 48.28, 109.70, 117.78, 119.60, 129.44, 133.35, 135.81, 137.58, 152.77, 172.89. ESI-MS m/z 273 $(M + H)^+$ calculated for $C_{16}H_{20}N_2O_2$.

*5-(n-Butylamino)-2-(2,5-dimethyl-1H-pyrrol-1-yl) benzoic acid (**3d**)*

Pale yellow oil (0.220 g, 77 %), $^1$H-NMR δ 0.85-0.88 (t, *J* = 7.2 Hz, 3H), 1.24-1.32 (m, 2H), 1.32-1.44 (m, 2H), 1.78 (s, 6H), 3.01-3.04 (t, *J* = 6.0 Hz, 2H), 5.64 (s, 2H), 6.07 (brs, 1H), 6.73-6.76 (dd, *J* = 7.6, 1.6 Hz, 1H), 6.88-6.90 (d, *J* = 8.4 Hz, 1H), 6.96-6.97 (d, *J* = 1.6 Hz, 1H), 12.49 (brs, 1H). $^{13}$C-NMR δ 13.05, 14.07, 20.00, 23.01, 42.86, 104.94, 112.60, 114.51, 124.87, 128.60, 131.00, 132.83, 149.96, 168.14. ESI-MS m/z 287 $(M + H)^+$ calculated for $C_{17}H_{22}N_2O_2$.

*5-(Cyclopropylamino)-2-(2,5-dimethyl-1H-pyrrol-1-yl) benzoic acid (**3e**)*

Pale yellow oil (0.203 g, 75 %), $^1$H-NMR δ 0.74-0.74 (d, *J* = 6.2 Hz, 4H), 1.76 (s, 6H), 3.71 (m, 1H), 5.65 (s, 2H), 6.95 (brs, 1H), 6.72-6.75 (dd, *J* = 8.4, 2.4 Hz, 1H), 6.88-6.90 (d, *J* = 8.4 Hz, 1H), 6.95-6.96 (d, *J* = 2.4 Hz, 1H), 12.52 (brs, 1H). $^{13}$C-NMR δ 17.81, 26.92, 48.27, 109.70, 117.78, 119.60, 129.44, 133.35, 135.81, 137.58, 152.78, 172.89. ESI-MS m/z 271 $(M + H)^+$ calculated for $C_{16}H_{18}N_2O_2$.

*5-(Cyclopropylmethylamino)-2-(2,5-dimethyl-1H-pyrrol-1-yl) benzoic acid (**3f**)*

Pale yellow oil (0.187 g, 66 %), $^1$H-NMR δ 0.12-0.15 (dd, *J* = 9.6, 4.4 Hz, 2H), 0.37-0.40 (dd, *J* = 7.6, 4.0 Hz, 2H), 0.87 (m, 1H), 1.79 (s, 6H), 2.89-2.92 (t, *J* = 6.4 Hz, 2H), 5.64 (s, 2H), 6.19 (brs, 1H), 6.76-6.79 (dd, *J* = 8.0, 1.6 Hz, 1H), 6.88-6.90 (d, *J* = 8.4 Hz, 1H), 6.97-6.98 (d, *J* = 2.0 Hz, 1H), 12.47 (brs, 1H). $^{13}$C-NMR δ 3.60, 11.25, 23.01, 43.27, 104.95, 112.60, 114.75, 124.94, 128.59, 130.97, 148.92, 164.14. ESI-MS m/z 285 $(M + H)^+$ calculated for $C_{17}H_{20}N_2O_2$.

*5-(Cyclohexylmethylamino)-2-(2,5-dimethyl-1H-pyrrol-1-yl) benzoic acid (**3g**)*

Pale yellow oil (0.187 g, 57 %), $^1$H-NMR δ 0.81-1.31 (m, 10H), 1.41 (m, 1H), 1.75 (s, 6H), 2.80-2.83 (t, *J* = 6.0 Hz, 2H), 5.60 (s, 2H), 6.08 (brs, 1H), 6.91-6.71 (d, *J* = 6.4 Hz, 1H), 6.82-6.51 (d, *J* = 8.8, 1H), 6.91-6.92 (d, *J* = 2.4 Hz, 1H), 12.43 (brs, 1H). $^{13}$C-NMR δ 18.89, 25.83, 37.87, 45.25 109.83, 112.10, 114.41, 124.13, 127.28, 130.82, 131.92, 149.21, 169.83. ESI-MS m/z 327 $(M + H)^+$ calculated for $C_{20}H_{26}N_2O_2$.



https://doi.org/10.58985/jddb.2024.v02i01.08

## 3. Results and Discussion

### *3.1 Computational part*

Receptor-based molecular modeling is an efficient computer-aided drug design technique that uses the structure of the target protein to identify novel leads. However, most methods consider protein flexibility and desolvation effects in a very approximate way, which may limit their use in practice [6]. Predicting relative protein–ligand binding affinities is a central pillar of lead optimization efforts in structure-based drug design. SILCS methodology is based on functional group affinity patterns in the form of free energy maps that may be used to compute protein–ligand binding poses and affinities [6]. SILCS-assisted molecular modeling protocol was introduced recently to address these issues, as SILCS naturally takes both protein flexibility and desolation effects into account by using full molecular dynamics (MD) simulations to determine 3D maps of the functional group-affinity patterns on a target receptor [6]. In the present work, simulations will be performed with CHARMM4 [7] using the CHARMM36 protein force field [8] and the CHARMM General Force Field for ligands [9]. SILCS MD simulations, FragMap generation, and calculation of LGFEs will be performed as previously described [10]. Docking of novel ligands into the SILCS FragMaps, as required to calculate LGFEs, will use the program AutoDock [11]. AutoDock allows for external "grids," in this case the SILCS FragMaps, to be read and used to direct ligand posing and scoring. LGFE predictions of relative free energy differences for selected ligands will be validated using free energy perturbation as implemented in the WCA approach [12]. A simplified flow diagram for the entire SILCS workflow yielding different qualitative and quantitative analyses is depicted in Figure 1 [10]. So as to achieve the best possible configuration, the SILCS-MC process begins with 10,000 steps of energy minimization of the ligand structure. This is followed by 10,000 steps of typical MC and 40,000 steps of annealing. For the standard MC, the temperature was set to 300 K, and for the annealing stages, it was progressively dropped to 0 K. The most advantageous LGFE scores, which are then utilized exclusively for ligand scoring, are employed to determine the final ligand binding conformations. For every ligand, we run five separate simulations that each needs at least 50 Monte Carlo (MC) runs. If the three most favorable

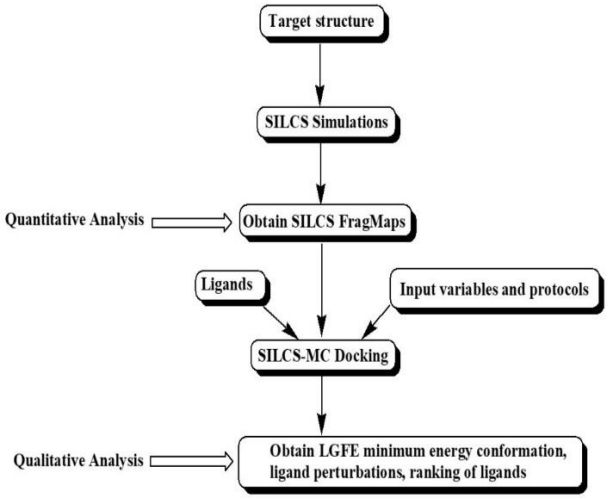


**Figure 1.** Flow diagram for the entire SILCS workflow [10].

LGFE scores were within 0.5 kcal mol-1 after 50 MC runs, the simulation was stopped; otherwise, it proceeded for a maximum of 250 MC runs before being stopped. This procedure was employed to enhance the overall sampling and find the minimum free energy binding conformation. The most favorable LGFE score and associated ligand conformation were then selected from the five independent simulations [10]. A new class of inhibitors (**3a-g**) for PTP1B will be designed by extending the chemical structure of with an additional hydrophobic group targeting the hydrophobic site next to the OH group of **P58** (Scheme 1). Motivated by this idea, the new inhibitors would: 1) keep the overall configuration and H-bonding potential of the OH group of **P58** and, 2) provide additional hydrophobic interactions that will interact favorably with PTP1B, and thus, further improve the potency of the inhibitors. The results from SILCS studies have shown that alternate hydrophobic motifs such as ethyl (**a**), propyl (**b**), isopropyl (**c**), n-butyl (**d**), cyclopropyl (**e**), cyclopropylmethyl (**f**), and cyclohexanylmethyl (**g**) may lead to improve binding. Additionally, a series of inhibitors **5-11** (Table 1) with a hydrophobic tail coupled to the carboxylic acid group of **P58** will be considered. SILCS modeling will be used to evaluate the feasibility of targeting the region next to the carboxylate of **P58**. Preliminary CADD using SILCS suggests that compounds **3a-g** will adopt a position and orientation similar to that of **P58** in its complex with PTP1B. To assess the specificity of the new inhibitors for PTP1B over other closely related enzymes including T-cell protein tyrosine phosphatase (TCPTP), all the designed


https://doi.org/10.58985/jddb.2024.v02i01.08

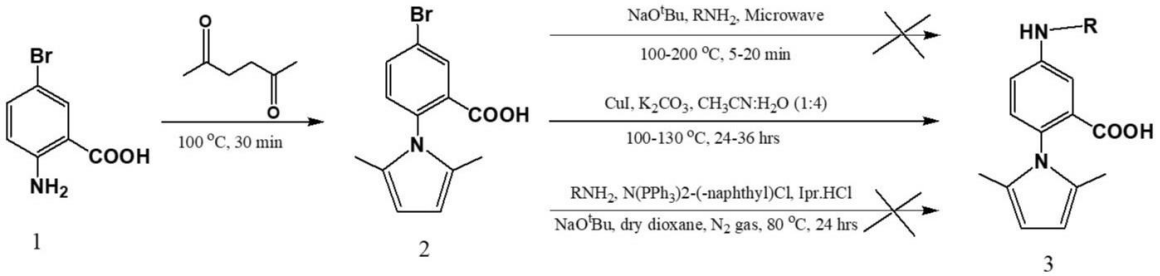


R = a = Ethyl, b = Propyl, c = Isopropyl, d = *n*-Butyl, e = Cyclopropyl, f = Cyclopropylmethyl, g = Cyclohexylmethyl

Scheme 1: General scheme for the synthesis of the target compouns **3a-g**

inhibitors (**P58, 2, 3a-g, and 4-11**) were also docked. The computational prediction results of the designed compounds (**P58, 2, 3a-g, and 4-11**) are presented in Table 1. The LGFE (generic and specific) of the designed compounds (**P58, 2, 3a-g, and 4-11**) indicated that the addition of the hydrophobic moiety to **P58** is much more favorable at position 5 than that of position 1. The most docked compound of the allosteric site of PTP 1B with highest LGFE (generic -24.883 kcal mol$^{-1}$ and specific -24.364 kcal mol$^{-1}$) was 5-(cyclopropylamino)-2-(2,5-dimethyl-1*H*-pyrrol-1-yl) benzoic acid **3e** while 5-(cyclohexylmethylamino)-2-(2,5-dimethyl-1*H*-pyrrol-1-yl) benzoic acid **3g** was the most docked one of TCPTP with LGFE (generic -25.414 kcal mol$^{-1}$ and specific -24.870 kcal mol$^{-1}$). The obtained results indicated the specificity and selectivity of **3e** to inhibit PTP 1B over closely related enzyme TCPTP where the LGFE of PTP 1B and TCPTP (generic difference) was -4.029 kcal mol$^{-1}$ and -7.075 kcal mol$^{-1}$, respectively (Table 1). Visualization of SILCS Fragmaps also reveals the favorable and unfavorable sites for functional group interactions throughout the allosteric site of PTP 1B (Fig. 2).

The molecular surface of the allosteric site of PTP 1B is shown in white while high-probability isosurfaces from the FragMaps are represented as meshes, with the aliphatic carbon FragMap in green, the aromatic carbon in purple, the hydrogen bond donor in blue, and hydrogen bond acceptor in red (Figure 2A). The hydrophobic pocket indicated by the green mesh is well overlapped by the cyclopropyl group in compound **3e** (Figure 2C) relative to Compound **P58**(Figure 2B). On the other hand, the hydrophobic

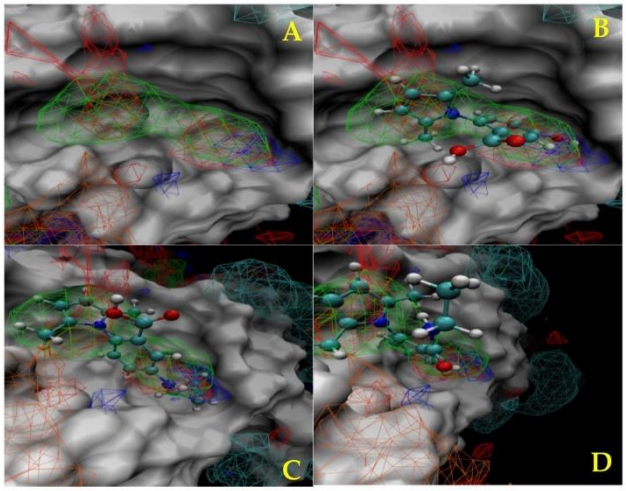


**Figure 2:** SILCS FragMaps for PTP 1B allosteric site are represented as meshes, with the aliphatic carbon FragMap in green, the aromatic carbon in purple, the hydrogen bond donor in blue, and the hydrogen bond acceptor in red. Ligand atoms are colored by element: (cyan) carbon, (red) oxygen, (blue) nitrogen, (pink) fluorine, and (white) hydrogen. A. PTP 1B allosteric site, B. PTP 1B docked with P58, C. PTP 1B docked with compound **3e**, D. PTP 1B docked with compound **5**.

pocket cannot be accommodated by even methyl group oriented at position 1 as presented in compound **5** (Figure 2D). The possible identification of therapeutic potentials of 5-(cyclopropylamino)-2-(2,5-dimethyl-1*H*-pyrrol-1-yl) benzoic acid **3e** which was confirmed through investigation in this study presents a positive insight into further confirmatory studies on its potential as a promising PTP 1B inhibitor and efforts are underway in this direction.

### *3.2 Chemistry part*

Previous SILCS methodology technique



https://doi.org/10.58985/jddb.2024.v02i01.08

investigations indicated that compounds **(3a-g)** as a good candidate for PTP1B inhibitors (previous section). The synthesis of the target compounds (**3a**-**e**) starts with 2-amino-5-bromobenzoic acid **1** (Scheme 1). Treatment of compound **1** with excess 2,5-hexanedione without solvent will yield 5-bromo-2-(2,5-Dimethyl-1*H*-pyrrol-1-yl) benzoic acid **2** [13]. The resulting bromobenzene derivative **2** will couple to various amines using catalysts developed by Ullmann to provide the targets (**3a**-**g**) [14-21]. Amination of aryl halides has been an important and frequently required reaction for the synthesis of a wide range of interesting molecules used in the pharmaceutical field [22]. The C-N cross-coupling of electron-deficient aryl halides is not accessed easily under mild conditions compared with the electron-rich ones [22]. In the past few years, the utilization of microwave irradiation in chemical transformation has attracted significant importance in the search for green chemistry. Trials to adopt a microwave condition as a rapid and direct amination of aryl halides without transition metal catalysis as reported for C-N formation of the final targets (**3a**-**g**) have failed [23]. Applying efficient nickel-catalyzed C-N coupling reactions since Ni (0) and Ni (II) reagents are used as Ni catalytically active sources and screening of the reaction conditions to afford the final targets (**3a**-**g**) are tried by using different ratios of trans-chloro(1-naphthyl)bis (tri-phenylphosphine)nickel (II) [Ni(PPh3)2-(1-naph)Cl] as catalyst and 1,3-bis(2,6-diisopropyl-phenyl) imi-dazolium chloride (Ipr.HCl) as legend but no reaction occurred [24]. The first direct synthesis of N-aryl derivatives from halobenzoic acid was accomplished by Ullmann [14-21]. However, stoichiometric copper concentrations, harsh reaction conditions, strong bases, and polar organic solvents are needed for the traditional Ullmann amination. Significant progress has been made in minimizing these issues, despite great efforts. Buchwald-Hartwig amination, which operates under milder conditions in the presence of palladium-based catalysts with phosphine ligands or N-heterocyclic carbenes, should be the most efficient substitute. It has been shown to be effective in studies [25-33]. The fact that these ligands are frequently costly, hazardous, and air-sensitive is a disadvantage to this amination process. As a result, the low cost and low toxicity of the copper-based Ullmann-type amination techniques attracted interest once more [25-33]. The optimized copper-catalyzed cross-coupling procedure for amination of 2-bromobenzoic acids using aliphatic amines was then applied to prepare desired products (**3a**-**g**) via a CuI catalyzed N-arylation of aryl halides using $K_2CO_3$ as a base [22]. Ullmann-type coupling of aryl halides with amines using copper is recognized as an economic and versatile method for rapidly accessing aryl amines. The structures of the synthesized targets (**3a-g**) are confirmed by IR, $^1$H, and $^{13}$C-NMR in addition to HR-MS.

## 4. Conclusion

The allosteric site of PTP 1B identified by the SILCS-Hotspots approach was applied to the ligand optimization of **P58**. These findings from this study established 5-(Cyclopropylamino)-2-(2,5-dimethyl-1*H*-pyrrol-1-yl) benzoic acid **3e** as a promising selective inhibitor of PTP 1B. The selective allosteric inhibition of **3e** strongly suggests it as a lead compound against PTP 1B for the management of T2DM. Further studies are imperative to focus on lead optimization as a novel PTP 1B inhibitor and efforts are underway in this direction.

## Acknowledgements

The author acknowledges Professor Alexander D. Mackerell Jr. at the Computer-Aided Drug Design (CADD) Center, University of Maryland, Baltimore, USA for the computer time and resources.

## Funding

This research received no external funding

## Availability of data and materials

All data will be made available on request according to the journal policy

## Conflicts of interest

No conflict of interest is associated with this work

## References

1. Hunter, T. Signaling-2000 and beyond. Cell. 2000, 100, 113-127. https://doi.org/10.1016/s0092-8674(00)81688-8.
2. Bialy, L.; Waldmann, H. Inhibitors of protein tyrosine phosphatases: next-generation drugs? Angewandte Chem. 2005, 44, 3814-3839. https://doi.org/10.1002/anie.200461517.

3. Wiesmann, C.; Barr, K.J.; Kung, J.; Zhu, J.; Erlanson, D.A.; Shen, W.; Fahr, B.J.; Zhong, M.; Taylor, L.; Randal, M.; McDowell, R.S.; Hansen, S.K. Allosteric inhibition of protein tyrosine phosphatase 1B. Nat. Struct. Mol. Biol. 2004, 11, 730-737. https://doi.org/10.1038/nsmb803.
4. Guvench, O.; MacKerell A.D. Computational Fragment-Based Binding Site Identification by Ligand Competitive Saturation. PLoS Comp. Biol. 2009, 5. e1000435. https://doi.org/10.1371/journal.pcbi.1000435.
5. MacKerell, A.D.; Jo, S.; Lakkaraju, S.K.; Lind, C.; Yu, W. Identification and characterization of fragment binding sites for allosteric ligand design using the site identification by ligand competitive saturation hotspots approach (SILCS-Hotspots). Biochim. Biophys. Acta. Gen. Subj. 2020, 1864, 129519-129558. https://doi.org/10.1016/j.bbagen.2020.129519.
6. Yu, W.; Lakkaraju, S.K.; Raman, E.P.; Fang, L.; MacKerell, A.D. Pharmacophore modeling using site-identification by ligand competitive saturation (SILCS) with multiple probe molecules. J. Chem. Inform. Model. 2015, 55, 407−420. https://doi.org/10.1021/ci500691p.
7. Brooks, B.R.; Brooks, C.L.; MacKerell, A.D.; Nilsson, L.; Petrella, R.J.; Roux, B.; Won, Y.; Archontis, G.; Bartel, C.; Boresch, S.; Caflisch, A.; Caves, L.; Cui, Q.; Dinner, A.R.; Feig, M.; Fischer, S.; Gao, J.; Hodoscek, M.; Im, W.; Kuczera, K.; Lazaridis, T.; Ma, J.; Ovchinnikov, V.; Paci, E.; Pastor, R.W.; Post, C.B.; Pu, J.Z.; Schaefer, M.; Tidor, B.; Venable, R.M.; Woodcock, H.L.; Wu, X.; Yang, W.; York, D.M.; Karplus, M.; CHARMM: The biomolecular simulation program. J. Comp. Chem. 2009, 30, 1545-1614. https://doi.org/10.1002/jcc.21287.
8. Best, R.B.; Zhu, X.; Shim, J.; Lopes, P.E.M.; Mittal, J.; Feig, M.; MacKerell, A.D. Optimization of the Additive CHARMM All-Atom Protein Force Field Targeting Improved Sampling of the Backbone $\phi$, $\psi$ and Side-Chain $\chi_1$ and $\chi_2$ Dihedral Angles. J. Chem. Theory and Comp. 2012, 8, 3257–3273. https://doi.org/10.1021/ct300400x.
9. Vanommeslaeghe, K.; Hatcher, E.; Acharya, C.; Kundu, S.; Zhong, S.; Shim, J.; Darian, E.; Guvench, O.; Lopes, P.; Vorobyov, I.; Mackerell, A.D. CHARMM general force field: A force field for drug-like molecules compatible with the CHARMM all-atom additive biological force fields. J. Comp. Chem. 2010, 31, 671-690. https://doi.org/10.1002/jcc.21367.
10. Goel, H.; Hazel, A., Ustach, V.D.; Jo, S.; YU, W.; Mackerell, A.D. Rapid and accurate estimation of protein–ligand relative binding affinities using site-identification by ligand competitive saturation. Chem. Sci. 2021, 12, 8844-8858. https://doi.org/10.1039/d1sc01781k.
11. Trott, O.; Olson, A.J. AutoDock Vina: Improving the speed and accuracy of docking with a new scoring function, efficient optimization, and multithreading. J. Comp. Chem. 2010, 31, 455-461. https://doi.org/10.1002/jcc.21334.
12. Deng, Y.; Roux, B. Hydration of amino acid side chains: nonpolar and electrostatic contributions calculated from staged molecular dynamics free energy simulations with explicit water molecules. J. Phys. Che. B. 2004, 108, 16567-16576. https://doi.org/10.1021/jp048502c.
13. Bradner, J.E.; McKeown, M.R.; Rahl, P.B.; Young, R.A.; Marineau, J.J. Pyrrol-1-yl benzoic acid derivatives useful as myc inhibitors. World Intellectual Property Organization, WO2014071247 A1 2014-05-08.
14. Gwilherm, E.; Nicolas, B.; Mathieu, T. Copper-mediated coupling reactions and their applications in natural products and designed biomolecules synthesis. Chem. Rev. 2008, 108, 3054–3131. https://doi.org/10.1021/cr8002505.
15. Ma, D.W.; Cai, Q. Copper/amino acid catalyzed cross-couplings of aryl and vinyl halides with nucleophiles. acc. Chem. Res. 2008, 41, 1450–1460. https://doi.org/10.1021/ar8000298.
16. Corbet, J.P.; Mignani, G. Selected patented cross-coupling reaction technologies. Chem. Rev. 2006, 106, 2651–2710. https://doi.org/10.1021/cr0505268.
17. Kienle, M.; Dubakka, S.R.; Brade, K.; Knochel P. Modern amination reactions. Eur. J. Org. Chem. 2007, 4166–4176. https://doi.org/10.1002/ejoc.200700391.
18. Carril, M.; SanMartin, R.; Dominguez, E. Palladium and copper-catalysed arylation reactions in the presence of water, with a focus on carbon–heteroatom bond formation. Chem. Soc. Rev. 2008, 37, 639–647. https://doi.org/10.1039/b709565c.
19. Scholz, U. Evolution of transition metal-catalyzed amination reactions: the industrial approach. Amino Group Chem. 2008, 333–363. https://doi.org/10.1002/9783527621262.ch9.
20. Das, P.; Sharma, D.; Kumar, M.; Singh, B. Copper promoted C-N and C-O type cross-coupling reactions. Curr. Org. Chem. 2010, 14, 754–783. https://doi.org/10.2174/138527210791111830.
21. Jiao, J.; Zhang, X-R.; Chang, N-H.; Wang, J.; Wei, Monnier, F.; Taillefer, M. Catalytic C-C, C-N, and C-O ullmann-type coupling reactions. Angew. Chem., Int. Ed. 2009, 48, 6954–6971. https://doi.org/10.1002/chin.200950227.
22. J-F.; Shi, X-Y.; Chen, Z-G. A Facile and practical copper powder-catalyzed, organic solvent- and ligand-free ullmann amination of aryl halides. J. Org. Chem. 2011, 76, 1180-1183. https://doi.org/10.1021/jo102169t.
23. Yadav, L.D.S.; Yadav, B.S.; Pai, V.K. Active-copper-promoted expeditious N-arylations in aqueous media under microwave irradiation. synthesis 2006, 11, 1868–1872. https://doi.org/10.1055/s-2006-942369.




https://doi.org/10.58985/jddb.2024.v02i01.08

24. Chen, C.; Yang, L-M. Ni (II) − (σ-Aryl) Complex: A Facile, efficient catalyst for nickel-catalyzed carbon−nitrogen coupling reactions. J. Org. Chem. 2007, 72, 6324–6327. https://doi.org/10.1021/jo0709448.
25. Surry, D.S.; Buchwald, S.L. Dialkylbiaryl phosphines in Pd-catalyzed amination: a user's guide. Chem. Sci. 2011, 2, 27–50. https://doi.org/10.1039/c0sc00331j.
26. Maiti, D.; Fors, B.P.; Henderson, J.L.; Nakamura, Y.; Buchwald, S.L. Palladium-catalyzed coupling of functionalized primary and secondary amines with aryl and heteroaryl halides: two ligands suffice in most cases. Chem. Sci. 2011, 2, 57–68. https://doi.org/10.1039/c0sc00330a.
27. Fors, B.P.; Watson, D.A.; Biscoe, M.R.; Buchwald, S.L. A highly active catalyst for Pd-catalyzed amination reactions: cross-coupling reactions using aryl mesylates and the highly selective monoarylation of primary amines using aryl chlorides. J. Am. Chem. Soc. 2008, 130, 13552–13554. https://doi.org/10.1021/ja8055358.
28. Sheng, Q.; Hartwig, J.F. [(CyPF-$^{t}$Bu) $PdCl_2$]: An air-stable, one-component, highly efficient catalyst for amination of heteroaryl and aryl halides. Org. Lett. 2008, 10, 4109–4112. https://doi.org/10.1021/ol801615u.
29. Reddy, C.V.; Kingston, J.V.; Verkade, J. $(t\text{-Bu})_2PN{=}P(i\text{-BuNCH}_2CH_2)_3N$: New efficient ligand for palladium-catalyzed C−N couplings of aryl and heteroaryl bromides and chlorides and for vinyl bromides at room temperature. Org. Chem. 2008, 73, 3047–3062. https://doi.org/10.1021/jo702367k.s010.
30. Slade, D.J.; Pelz, N.F.; Bodnar, W.; Lampe, J.W.; Watson, P.S. Indazoles: Regioselective protection and subsequent amine coupling reactions. J. Org. Chem. 2009, 74, 6331–6334. https://doi.org/10.1021/jo9006656.
31. Doherty, S.; Smyth, C.H.; Harrington, R.W.; Clegg W. Synthesis of biaryl diphosphines via a stepwise regioselective double diels−alder cycloaddition−elimination sequence: efficient ligands for the palladium-catalyzed amination of aromatic bromides. Organometallics. 2009, 28, 5273–5276. https://doi.org/10.1021/om9004862.
32. Vo, G.D.; Hartwig J.F. Palladium-catalyzed coupling of ammonia with aryl chlorides, bromides, iodides, and sulfonates: a general method for the preparation of primary arylamines. J. Am. Chem. Soc. 2009, 131, 11049–11061. https://doi.org/10.1021/ja903049z.
33. Schultz, D.M.; Wolfe, J.P. Synthesis of polycyclic nitrogen heterocycles via alkene aminopalladation/carbopalladation cascade reactions. Org. Lett. 2010, 12, 1028–1031. https://doi.org/10.1021/ol100033s.


https://doi.org/10.58985/jddb.2024.v02i01.08